STUDY OF CRITICAL BEHAVIOR IN $Fe_{88}Co_2Zr_7B_2Cu_1$ ALLOY RIBBONS

Nguyen Hai Yen[a, b*], Nguyen Hoang Ha[b, c], Pham Thi Thanh[a, b], Kieu Xuan Hau[a], Tran Dang Thanh[a, b], Nguyen Huy Dan[a, b]

[a]*Institute of Materials Science, Vietnam Academy of Science and Technology, Hanoi, Vietnam*
[b]*Graduate University of Science and Technology, Vietnam Academy of Science and Technology, Hanoi, Vietnam*
[c]*Lam Son Gifted High School, Thanh Hoa, Vietnam*
[*]*Corresponding author: Email: yennh@ims.vast.ac.vn*

Article history
Received: March 11th, 2021
Received in revised form: May 18th, 2021 | Accepted: May 21st, 2021
Available online: May 31st, 2021

Abstract

In this work, we investigated the critical behavior of $Fe_{88}Co_2Zr_7B_2Cu_1$ alloy ribbons prepared using a single-roller melt-spinning method. X-ray diffraction analysis shows that the alloy is almost amorphous. This alloy undergoes a second-order ferromagnetic-paramagnetic (FM-PM) phase transition at room temperature (Curie temperature T_C = 296 K). To investigate the nature of the FM-PM phase transition near the T_C for the alloy, we performed a critical-exponent study. Based on modified Arrott plots, the Kouvel-Fisher method, and Widom's scaling relation, a set of critical parameters were determined. The critical parameters are $\beta = 0.545 \pm 0.041$ and $\gamma = 1.109 \pm 0.018$ obtained from the modified Arrott plots; $\beta = 0.547 \pm 0.005$ and $\gamma = 1.105 \pm 0.016$ from the Kouvel-Fisher method, and $\delta = 3.035 \pm 0.059$ from Widom's scaling relation. These values are close to those expected for the mean-field model, revealing long-range FM interactions.

Keywords: Critical parameter; Magnetic entropy change; Magnetic refrigeration; Magnetic transition; Magnetocaloric effect; Melt-spinning method.

DOI: http://dx.doi.org/10.37569/DalatUniversity.11.4.869(2021)

Article type: (peer-reviewed) Full-length research article

1. INTRODUCTION

The magnetocaloric effect (MCE) of magnetic materials near room temperature is increasingly of research interest because of its applicability in magnetic refrigeration (MR), a more efficient and environmentally friendly technique than the conventional gas technique (Franco et al., 2018; Gschneidner et al., 2005). The MCE is the change in temperature of a magnetic material under a change in an external magnetic field in an adiabatic process. This effect can be evaluated through its magnetic entropy change (ΔS_m) and refrigerant capacity (RC). In the conventional gas technique, pure Gd metal is used as a typical magnetic refrigerant for MR in the room temperature region because it exhibits a large MCE around the Curie temperature T_C = 294 K (Dunhui et al., 2005; Gschneidner et al., 2005). However, the expense of Gd has limited its application. In recent years, some materials with a large magnetocaloric effect have been found, such as Ni-Mn based Heusler alloys (Dadda et al., 2020; Ghosh & Ghosh, 2020), Gd-containing alloys (Duc et al., 2019; Dunhui et al., 2005), Fe-Zr based alloys (Chen et al., 2018; Wang et al., 2020a), La-containing alloys (Mañosa et al., 2011; L. Yang et al., 2020), and the ferromagnetic perovskite manganites (Bouzidi et al., 2020; Phan & Yu, 2007). Among these materials, the Fe-Zr-based alloys have been the focus of research for the following reasons: (1) large magnetocaloric effect over a wide temperature range; (2) high resistivity, good mechanical properties, and no toxicity; (3) low price of Fe and Zr metals; and (4) their *T*c can be easily adjusted in the temperature range from 250 K to 350 K by adding other elements to their alloys (Chaudhary et al., 2019; Chen et al., 2018; Wang et al., 2020a). Therefore, these Fe-Zr-based alloys are very suitable for room temperature magnetic refrigeration.

In our previous study of $Fe_{90-x}Co_xZr_7B_2Cu_1$ (x = 0, 1, 2, 3, and 4) alloy ribbons (Yen et al., 2019a), we found that $Fe_{88}Co_2Zr_7B_2Cu_1$ alloy had the highest MCE (maximum entropy change $|\Delta S_m|_{max}$ = 0.82 J.kg^{-1}.K^{-1} and RC = 130 J.kg^{-1} with ΔH = 12 kOe) with T_C at room temperature. These characteristics reveal the potential application of $Fe_{88}Co_2Zr_7B_2Cu_1$ alloy ribbons for room-temperature magnetic refrigeration. Therefore, in this work, to further understand the magnetic properties of this alloy, we have investigated the critical behavior of $Fe_{88}Co_2Zr_7B_2Cu_1$ around its T_C using modified Arrott plots (Arrott & Noakes, 1967), Kouvel-Fisher (Kouvel & Fisher, 1964) methods, and Widom's scaling relation (Widom, 1964).

2. EXPERIMENTAL

Alloy with a nominal composition of $Fe_{88}Co_2Zr_7B_2Cu_1$ was prepared from Fe, Co, Zr, B, and Cu metals with 99.9% purity. First, an alloy ingot was fabricated in an argon environment using an arc-melting furnace. To ensure homogeneity, the sample was arc-melted several times. After that, the resulting arc-melted ingot was used to fabricate alloy ribbons by the melt-spinning method on a single roller apparatus. The quenching rate can be chosen by changing the velocity of the roller. In this work, the alloy ribbons were prepared with the highest roller velocity, v = 40 m/s. The ribbons we obtained have a thickness of about 30 μm. The structure of the ribbons at room temperature was examined by x-ray diffraction (XRD) with an EQUINOX 5000 diffractometer (Thermo Scientific,

France) and a Cu K-α radiation source (λ = 1.5406 Å). All magnetization measurements versus the temperature and magnetic field were carried out using a vibrating sample magnetometer with a maximum magnetic field of 12 kOe and a temperature range of 100-400 K.

3. RESULTS AND DISCUSSION

The structure of the alloy ribbons was examined by the powder X-ray diffraction (XRD) method. Figure 1 is the XRD pattern of a $Fe_{88}Co_2Zr_7B_2Cu_1$ ribbon measured at room temperature. The result shows that there is only a broad diffraction peak of low intensity. This proves that the alloy is almost amorphous. Similar results have been found in many other Fe-Zr-based amorphous alloys, such as $Fe_{88-x}Sm_xZr_8B_4$ (Chen et al., 2018), $Fe_{92-x}B_xZr_{10}$ (Wang et al., 2020b), and $Fe_{91-x}Cu_xZr_9$ (W. Yang et al., 2020).

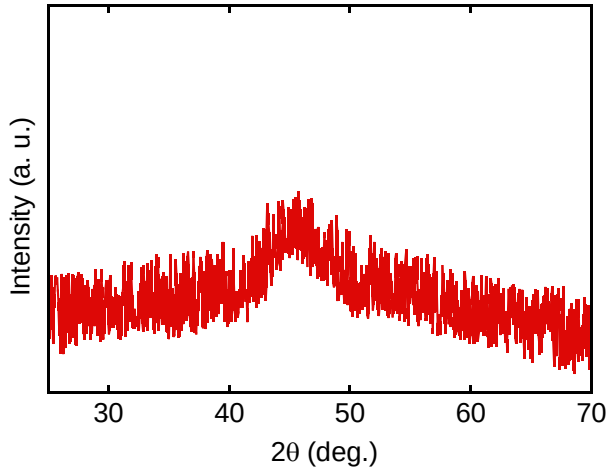

Figure 1. XRD pattern of $Fe_{88}Co_2Zr_7B_2Cu_1$ alloy ribbons

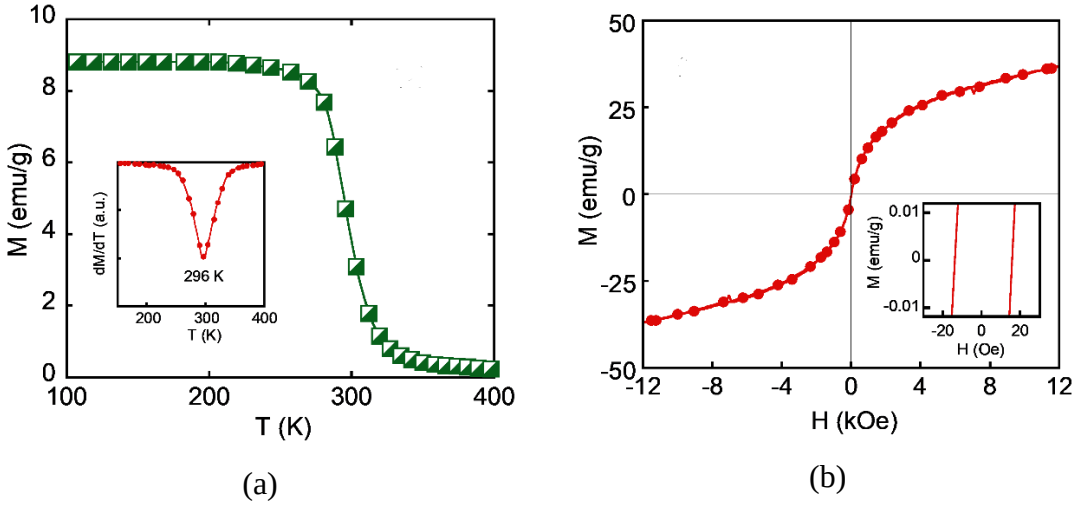

Figure 2. *M*(T) curve with *H* =100 Oe (a) and *M(H)* loop at room temperature (b) of $Fe_{88}Co_2Zr_7B_2Cu_1$ alloy ribbons

Figure 2a displays the thermomagnetic curve, $M(T)$, for $Fe_{88}Co_2Zr_7B_2Cu_1$ ribbons measured in an applied magnetic field of H = 100 Oe. From this figure, we can see that the $M(T)$ curve presents a broadened ferromagnetic-to-paramagnetic (FM-PM) phase transition. The Curie temperature, T_C, calculated by taking the minimum of the derivative dM/dT plot (see insert in Figure 2a), is 296 K. It should be noted that the T_C of $Fe_{88}Co_2Zr_7B_2Cu_1$ alloy ribbons is significantly higher than those of $Fe_{90}Zr_7B_2Cu_1$ (T_C = 245 K) (Yen et al., 2019b) and $Fe_{88}Zr_7B_4Cu_1$ ribbons (T_C = 287 K) (Chaudhary et al., 2019) without Co-doping. With the addition of Co, the ferromagnetic interactions are further enhanced (Gan et al., 2017; Li et al., 2018). This leads to the increment of the T_C having an important role in adjusting the working temperature of magnetic refrigerants.

The hysteresis loop, $M(H)$, of the $Fe_{88}Co_2Zr_7B_2Cu_1$ alloy ribbons measured at room temperature is displayed in Figure 2b. One can see that this hysteresis loop represents a common characteristic of ferromagnetic materials when it is measured at temperatures near the phase transition. The loop is almost unsaturated in the high magnetic field region. With an increase in H, the magnetization increases rapidly. At H = 12 kOe, the maximum magnetization, $M_{12\ kOe}$, is 37.1 emu/g. The coercivity H_c is found to be 15.2 Oe (see insert in Figure 2b), resulting in small magnetic hysteresis effect and therefore profitable for active magnetic refrigeration.

To further clarify the characteristics of the magnetic transition, we determined the magnetic field dependence of the magnetization, $M(H, T)$, at various temperatures (using a 2-K interval) around the FM-PM magnetic phase transition, as presented in Figure 3. It appears that at a given magnetic field, the magnetization, M, decreases with increasing temperature, T. For temperatures below the T_C, M increases sharply in the weak magnetic field region and then increases gradually in the stronger field region.

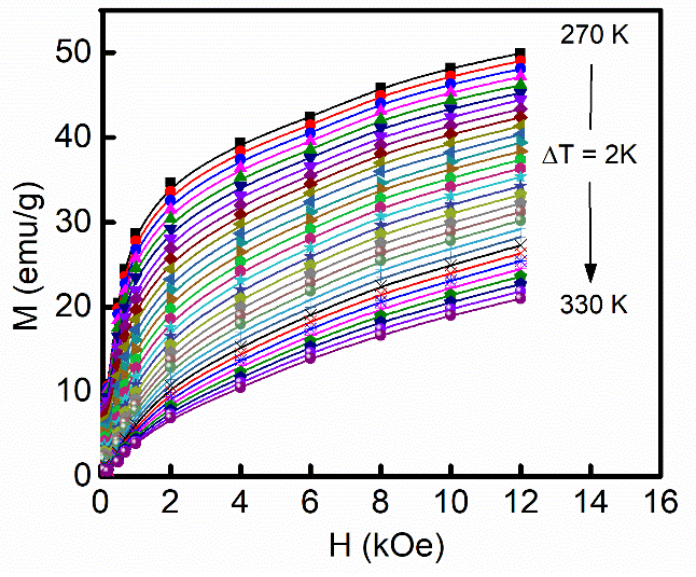

Figure 3. *M(H, T)* curves of $Fe_{88}Co_2Zr_7B_2Cu_1$ alloy ribbons around the FM-PM magnetic phase transition temperature

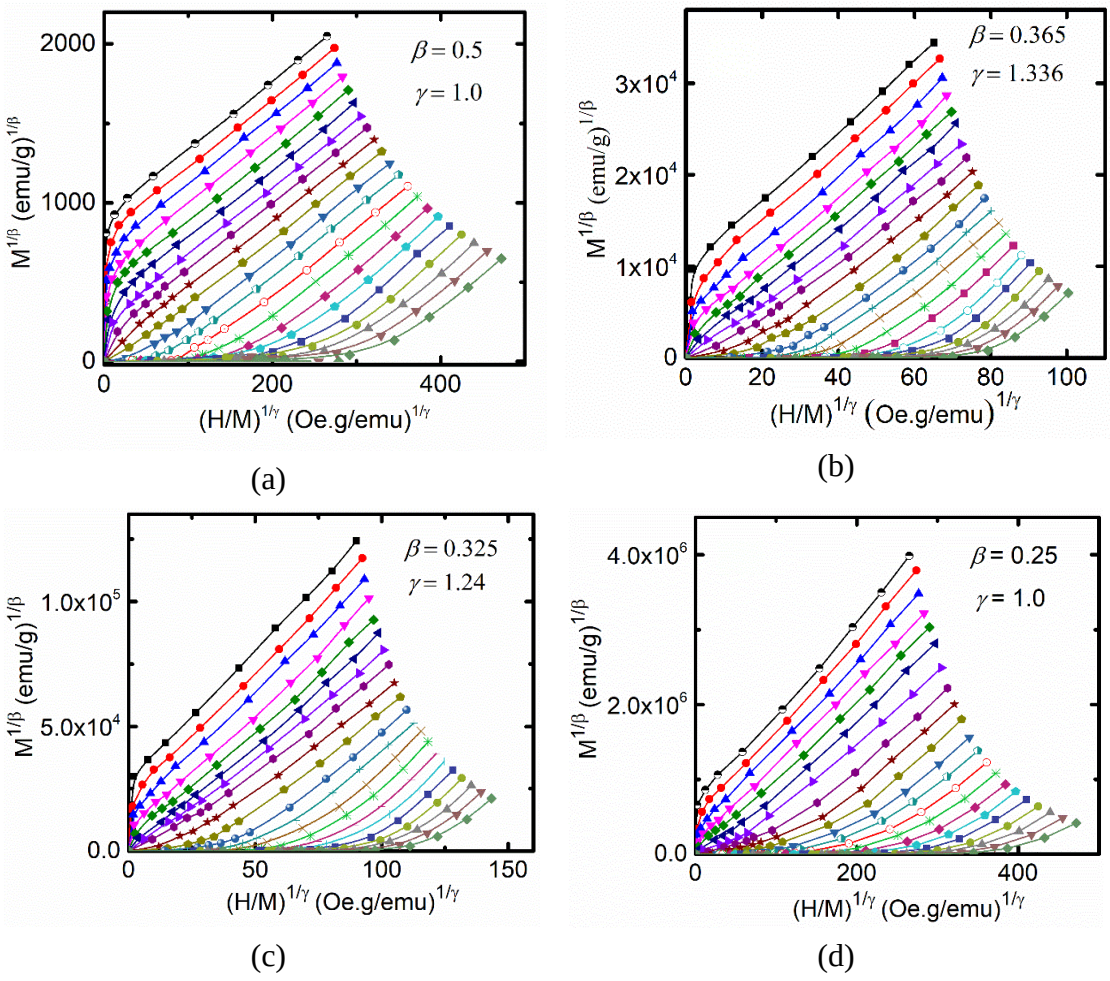

Figure 4. Modified Arrott plots: isothermal of $M^{1/\beta}$ versus $(H/M)^{1/\gamma}$ with the mean-field model (a), 3D Heisenberg model (b), 3D Ising model (c), and tricritical mean-field model (d) for $Fe_{88}Co_2Zr_7B_2Cu_1$ alloy ribbons

To accurately analyze the nature of the magnetic phase and magnetic orders in the alloy ribbons based on the $M(H, T)$ data, Arrott plots (M^2-H/M) were constructed for the $Fe_{88}Co_2Zr_7B_2Cu_1$ alloy ribbons within the temperature range from 280 K to 320 K (Figure 4a). According to Banerjee's criteria (Banerjee, 1964), the sign of the slope of the Arrott curves indicates the order of the phase transition. A material will undergo a second-order magnetic phase transition (SOMPT) if the slope of the M^2-H/M curves is positive. Conversely, a negative slope for the M^2-H/M curves corresponds to a first-order magnetic phase transition (FOMPT). As shown in Figure 4a, all the M^2-H/M curves of the $Fe_{88}Co_2Zr_7B_2Cu_1$ alloy ribbons have a positive slope, revealing the second-order nature of their magnetic phase transition.

In addition, the nature of the FM interactions in the material can be studied by examining critical behavior. The critical behavior of a SOMPT material is characterized by a set of critical parameters, β, γ, and δ, that are associated with the temperature dependence of spontaneous magnetization $M_S(T)$, the inverse initial susceptibility $\chi_0^{-1}(T)$,

and the magnetization isotherm at the T_C, respectively. These parameters can be determined from the following relations (Arrott & Noakes, 1967):

$$M_s(T) = M_0(-\varepsilon)^{\beta}, \qquad \varepsilon < 0 \tag{1}$$

$$\chi_0^{-1} = (H_0/M_0)\varepsilon^{\gamma}, \qquad \varepsilon > 0 \tag{2}$$

$$H = DM^{1/\delta}, \qquad \varepsilon = 0 \tag{3}$$

where $\varepsilon = (T - T_C)/T_C$ is the reduced temperature and M_o, h_o/M_o, and D are critical amplitudes. With the true values of β and γ, the $M^{1/\beta}$-$(H/M)^{1/\gamma}$ curves in the high magnetic region are a group of parallel straight lines, for which the line at $T = T_C$ must pass through the coordinate origin.

To determine the critical parameters for the amorphous $Fe_{88}Co_2Zr_7B_2Cu_1$ alloy, we analyzed the $M(H, T)$ data around the T_C by using the modified Arrott plot (MAP) method (Arrott & Noakes, 1967). Figure 4 presents MAPs for the alloy ribbons constructed using four theoretical exponential models: the mean-field model (Figure 4a), the 3D Heisenberg model (Figure 4b), the 3D Ising model (Figure 4c), and the tricritical mean-field model (Figure 4d). One can see that in the high magnetic field region, all lines for the models are almost parallel to each other, except for the curves in Figure 4d. To find the most suitable model for the ribbons, we determined the relative slopes (RS) of these lines. The RS is defined as the ratio between the slope of the quasi-straight line in the high field region at T (S(T)) and T_C (S(T_C)), i.e., RS = S(T)/S(T_C). The RS of the most suitable model will be approximately equal to 1, irrespective of temperature (Castaño et al., 1999). Figure 5 shows the temperature dependence of the relative slope RS(T) for the four models. From this figure, it appears that the RS values of the mean-field model are closer to unity than the other models for the $Fe_{88}Co_2Zr_7B_2Cu_1$ alloy ribbons. Therefore, the mean-field model is the most suitable model for determining the critical exponents of the alloy.

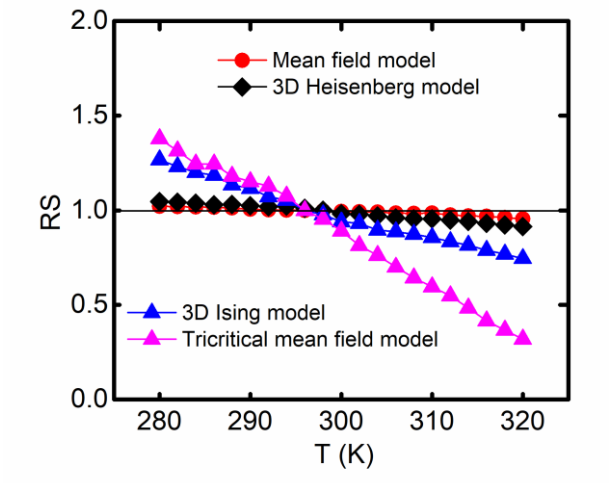

Figure 5. Temperature dependence of the relative slope RS for $Fe_{88}Co_2Zr_7B_2Cu_1$ alloy ribbons

We used $\beta = 0.5$ and $\gamma = 1.0$ as the initial trial values for further calculations. The $M_S(T)$ and $\chi_0^{-1}(T)$ can be obtained from the intersection of the linear extrapolation of the $M^{1/\beta}$-$(H/M)^{1/\gamma}$ curves with $M^{1/\beta}$ and the $(H/M)^{1/\gamma}$ axis in the high field region, respectively. Then, by fitting the $M_S(T)$ and $\chi_0^{-1}(T)$ data to Equations 1 and 2, the values β, γ, and T_C were estimated. Using the new β and γ values, this procedure was repeated until the critical exponents β and γ do not change and the $M^{1/\beta}$-$(H/M)^{1/\gamma}$ curve is a parallel straight line that passes through the coordinate origin. The final fitted curves are presented in Figure 6a. The critical parameters are found to be $\beta = 0.545 \pm 0.041$ at $T_C = 296.7$ K $\pm$ 0.142 (from Equation 1) and $\gamma = 1.109 \pm 0.018$ at $T_C = 296.9$ K $\pm$ 0.176 (from Equation 2). Based on the statistical theory, the δ parameter can be specified through Widom's scaling relation (Widom, 1964): $\delta = 1 + \gamma/\beta$. The result for the value of δ is 3.035 $\pm$ 0.059. These critical parameters are very close to those expected for the mean-field theory of long-range ferromagnetic orders (Stanley, 1972). Other Fe-Zr-based amorphous alloys also show long-range FM interactions, such as $Fe_{77}Co_{5.5}Ni_{5.5}Zr_7B_4Cu$ (Franco et al., 2011), $Fe_{82-x}Cr_{4+x}B_2Gd_2Zr_{10}$ (Yen et al., 2019b), $Fe_{85}Ni_5Zr_{10}$ (Thanh et al., 2014), and $(Fe_{0.74}Cu_{0.26})_{85}Zr_{15}$ (Castaño et al., 1999). Moreover, it should be noted that this T_C for the alloy ribbons is nearly equal to that directly determined from the minimum of the dM/dT versus T curve, meaning that the procedures for fitting and reducing the data are correct.

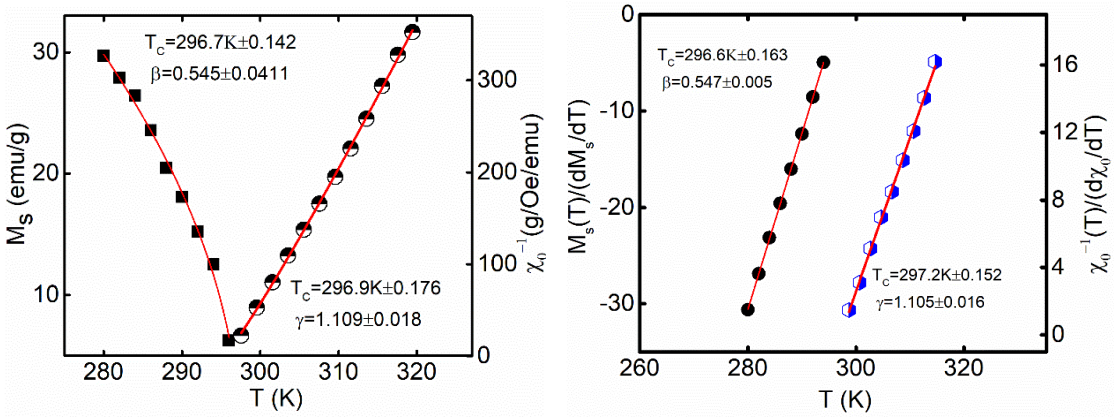

(a) (b)

Figure 6. Temperature dependence of $M_S(T)$ and $\chi_0^{-1}(T)$ along with fits to the Arrott-Noakes relations (a) and Kouvel-Fisher plots (b) for $Fe_{88}Co_2Zr_7B_2Cu_1$ ribbons

The Kouvel-Fisher method is also an accurate way of obtaining the critical parameters β and γ (Kouvel & Fisher, 1964). This method reformulates Equations 1 and 2 as the following:

$$M_S(T)[dM_S/dT]^{-1} = (T - T_C)/\beta \quad (4)$$

$$\chi_0^{-1}(T)[d\chi_0^{-1}(T)/dT]^{-1} = (T - T_C)/\gamma \quad (5)$$

The temperature dependence of $M_S(T)/(dM_S(T)/dT)$ and $\chi_0^{-1}(T)/(d\chi_0^{-1}(T)/dT)$ determined by this method are displayed in Figure 6b. The linear fits to the Kouvel-Fisher plots give the critical parameters. As a result, the critical parameters for the

$Fe_{88}Co_2Zr_7B_2Cu_1$ alloy ribbons are $\beta = 0.547 \pm 0.005$, $\gamma = 1.105 \pm 0.016$, and $T_C = 297.2$ K $\pm$ 0.2. Therefore, it can be seen that the critical parameters determined from the Kouvel-Fisher method almost coincide with those determined from the MAP method. This proves that the calculated critical parameters are reliable.

4. CONCLUSION

The structure, magnetic properties, and critical behavior of $Fe_{88}Co_2Zr_7B_2Cu_1$ alloy ribbons were studied in this work. The alloy ribbons undergo a second-order magnetic transition from PM to FM phase around their Curie temperature T_C = 296 K (room temperature). The critical parameters ($\beta = 0.545 \pm 0.041$, $\gamma = 1.109 \pm 0.018$, and $\delta = 3.035 \pm 0.059$) are close to those expected for the mean-field theory, indicating that the FM interactions are long-range.

ACKNOWLEDGMENTS

This research is funded by Vietnam National Foundation for Science and Technology Development (NAFOSTED) under grant number 103.02-2018.340. Part of the work was done at Key Laboratory for Electronic Materials and Devices, and Laboratory of Magnetism and Superconductivity, Institute of Materials Science, Vietnam.

REFERENCES

Arrott, A., & Noakes, J. E. (1967). Approximate equation of state for nickel near its critical temperature. *Physical Review Letters, 19*(14), 786-789.

Banerjee, B. K. (1964). On a generalised approach to first and second order magnetic transitions. *Physics Letters, 12*, 16-17.

Bouzidi, S., Gdaiem, M. A., Rebaoui, S., Dhahri, J., & Hlil, E. K. (2020). Large magnetocaloric effect in $La_{0.75}Ca_{0.25-x}Na_xMnO_3$ ($0 \leq x \leq 0.10$) manganites. *Applied Physics A, 126*(1), 60.

Castaño, F. J., García-Beneytez, J. M., Crespo, P., Multigner, M., Vazquez, M., & Hernando, A. (1999). Static critical phenomena in ball milled $(Fe_{0.74}Cu_{0.26})_{85}Zr_{15}$ amorphous alloy. *Journal of Physics: Condensed Matter, 11*(29), 5671-5680.

Chaudhary, V., Chen, X., & Ramanujan, R. V. (2019). Iron and manganese based magnetocaloric materials for near room temperature thermal management. *Progress in Materials Science, 100*, 64-98.

Chen, L., Zhang, J., Wen, L., Yu, P., & Xia, L. (2018). Outstanding magnetocaloric effect of $Fe_{88-x}Zr_8B_4Sm_x$ (x = 0, 1, 2, 3) amorphous alloys. *Science China Physics, Mechanics & Astronomy, 61*(5), 056121.

Dadda, K., Alleg, S., Suñol, J. J., Bessais, L., & Hlil, E. K. (2020). Structure, magnetocaloric effect and critical behaviour in $Ni_{50}Mn_{30}(Sn,In)_{20}$ Heusler alloys. *Journal of Superconductivity and Novel Magnetism, 33*(7), 2209-2218.

Duc, N. T. M., Shen, H. X., Clements, E. M., Thiabgoh, O., Sanchez Llamazares, J. L., Sanchez-Valdes, C. F., Huong, N. T., Sun, J. F., Srikanth, H., & Phan, M. H. (2019). Enhanced refrigerant capacity and Curie temperature of amorphous $Gd_{60}Fe_{20}Al_{20}$ microwires. *Journal of Alloys and Compounds, 807*, 151694.

Dunhui, W., Zhida, H., Qingqi, C., Songling, H., Jianrong, Z., & Youwei, D. (2005). The reduced Curie temperature and magnetic entropy changes in $Gd_{1-x}In_x$ alloys. *Journal of Alloys and Compounds, 396*(1), 22-24.

Franco, V., Blázquez, J. S., Ipus, J. J., Law, J. Y., Moreno-Ramírez, L. M., & Conde, A. (2018). Magnetocaloric effect: From materials research to refrigeration devices. *Progress in Materials Science, 93*, 112-232.

Franco, V., Caballero-Flores, R., Conde, A., Knipling, K. E., & Willard, M. A. (2011). Magnetocaloric effect and critical exponents of $Fe_{77}Co_{5.5}Ni_{5.5}Zr_7B_4Cu_1$: A detailed study. *Journal of Applied Physics, 109*(7), 07A905.

Gan, L., Ma, L., Tang, B., Ding, D., & Xia, L. (2017). Effect of Co substitution on the glass forming ability and magnetocaloric effect of $Fe_{88}Zr_8B_4$ amorphous alloys. *Science China Physics, Mechanics & Astronomy, 60*, 076121.

Ghosh, S., & Ghosh, S. (2020). Cosubstitution in Ni-Mn-Sb Heusler compounds: Realization of room-temperature reversible magnetocaloric effect driven by second-order magnetic transition. *Physical Review Materials, 4*(2), 025401.

Gschneidner, K. A. Jr., Pecharsky, V. K., & Tsokol, A. O. (2005). Recent developments in magnetocaloric materials. *Reports on Progress in Physics, 68*(6), 1479-1539.

Kouvel, J. S., & Fisher, M. E. (1964). Detailed magnetic behavior of nickel near its Curie point. *Physical Review, 136*(6A), A1626-A1632.

Li, X., Pan, Y., & Lu, T. (2018). Magnetocaloric effect in Fe-based amorphous alloys and their composites with low boron content. *Journal of Non-Crystalline Solids, 487*, 7-11.

Mañosa, L., González-Alonso, D., Planes, A., Barrio, M., Tamarit, J. -L., Titov, I. S., Acet, M., Bhattacharyya, A., & Majumdar, S. (2011). Inverse barocaloric effect in the giant magnetocaloric La-Fe-Si-Co compound. *Nature Communications, 2*(1), 595.

Phan, M. -H., & Yu, S. -C. (2007). Review of the magnetocaloric effect in manganite materials. *Journal of Magnetism and Magnetic Materials, 308*(2), 325-340.

Stanley, H. E. (1972). Introduction to phase transitions and critical phenomena. *American Journal of Physics, 40*(6), 927-928.

Thanh, T. D., Dan, N. H., Phan, T. -L., Kumarakuru, H., Olivier, E. J., Neethling, J. H., & Yu, S. -C. (2014). Critical behavior of the ferromagnetic-paramagnetic phase transition in $Fe_{90-x}Ni_xZr_{10}$ alloy ribbons. *Journal of Applied Physics, 115*(2), 023903.

Wang, X., Wang, Q., Tang, B. Z., Ding, D., Cui, L., & Xia, L. (2020a). Magnetic and magneto-caloric properties of the amorphous $Fe_{92-x}Zr_8B_x$ Ribbons. *Materials, 13*(23), 5334.

Wang, X., Wang, Q., Tang, B. Z., Ding, D., Cui, L., & Xia, L. (2020b). Magnetic and magneto-caloric properties of the amorphous $Fe_{92-x}Zr_8B_x$ ribbons. *Materials (Basel, Switzerland), 13*(23), 5334.

Widom, B. (1964). Degree of the critical isotherm. *The Journal of Chemical Physics, 41*(6), 1633-1634.

Yang, L., Li, J., Tu, D., Strickland, J. C. J., Hu, Q., Dong, H., & Li, J. (2020). Reduced annealing time and enhanced magnetocaloric effect of $La(Fe, Al)_{13}$ alloy by La-nonstoichiometry and Si-doping. *Acta Metallurgica Sinica (English Letters), 33*(11), 1535-1542.

Yang, W., Li, W., Wan, C., Huo, J., Mo, J., Liu, H., & Shen, B. (2020). Low-temperature magnetic properties and magnetocaloric effect of Fe-Zr-Cu amorphous alloys. *Journal of Low Temperature Physics, 200*(1), 51-61.

Yen, N. H., Ha, N. H., Thanh, P. T., Ngoc, N. H., Thanh, T. D., & Dan, N. H. (2019a). *Magnetic properties and magnetocaloric effect of* $Fe_{90-x}Co_xZr_7Cu_1B_2$ *rapidly quenched alloys* [Paper presentation]. The 4th International Conference on Advanced Materials and Nanotechnology (ICAMN), Hanoi, Vietnam.

Yen, N. H., Ha, N. H., Thanh, P. T., Thanh, T. D., Ngoc, N. H., & Dan, N. H. (2019b). Influence of Cr-addition on magnetic properties and magnetocaloric effect of Fe-Cr-B-Gd-Zr rapidly quenched alloys. *Journal of Electronic Materials, 48*(11), 7282-7291.